ADVANCED FUNCTIONAL MATERIALS
www.afm-journal.de

Enhanced Specificity in Capturing and Restraining Circulating Tumor Cells with Dual Antibody–Dendrimer Conjugates

Jingjing Xie, Yusheng Lu, Haiyan Dong, Rongli Zhao, Hongning Chen, Weiyu Shen, Patrick J. Sinko, Yewei Zhu, Jichuang Wang, Jingwei Shao, Yu Gao, Fangwei Xie, and Lee Jia**

Specifically capturing and restraining residual circulating tumor cells (CTCs) in cancer patients are the sine qua non for safely and effectively preventing cancer metastasis, to which the current chemotherapy has been limited due to its toxicity. Moreover, because of CTCs' rarity and low activity, the current technology for capturing CTCs based solely on a single surface biomarker has limited capacity and is used mainly for in vitro diagnosis. Here, it is possible to sequentially conjugate two CTCs antibodies (aEpCAM and aSlex) to the functionalized dendrimers to specifically capture human hepatocellular CTCs in both artificial and clinical patient blood samples, and restrain their activities. The molecular entities of the conjugates are demonstrated by various means. The dual antibody conjugate captured CTCs threefold more than the single counterparts from the high concentrations of interfering red blood cells or leukocytes, as well as from the blood of liver cancer patients, and exhibits the superiority to their single counterparts in down-regulating the captured CTCs. These results collectively provide the strong evidence that two antibodies can be compatibly conjugated to a nanomaterial, resulting in an enhanced specificity in restraining CTCs in blood.

1. Introduction

Cancer metastasis is a serious social, economic, and scientific problem world-wide that needs an urgent solution. As the estimated number of cancer survivors will reach 18 millions in the USA alone by 2022,[1] the cancer metastasis chemoprevention program becomes increasingly important and badly needs to prevent cancer metastasis after surgical removal of primary cancer. The root cause of cancer metastasis is presumably related to the residual circulating tumor cells (CTCs) in blood of asymptomatic cancer survivors.[2] Owing to their low proliferation rate and rarity,[3] the current post-metastatic chemotherapy that targets high proliferative cell lines can be ineffective in targeting and killing cancer cells specifically.[4] In fact, the anticancer chemotherapy may enhance metastasis formation.[5] Current bionanotechnology has utilized a single CTCs surface biomarker antibody such as the anti-epithelial cell adhesion molecule (anti-EpCAM) to coat silicon-nanopillar,[6] nanoscale poly(amidoamine) (PAMAM) dendrimers[7] or functionalized grapheme oxide nanosheets[8] for capturing CTCs in vitro for diagnostic purpose only.

The current nanotechnology for recognizing and binding the rare CTCs is mainly designed to enhance the local topographic interaction[6,9] between bionanomaterial conjugates (composed of a chemotherapeutic drug and a targeting antibody) and surface biomarkers of the typical CTCs, and is delimited to the low capability and specificity of binding and capturing CTCs. Human CTCs may possess more than one surface biomarker.[10] The abundance of a single surface biomarker may also fluctuate with the change of cell cycle phase resulting in variable binding affinity between the biomarker and its corresponding targeting antibody.[11] CTCs can undergo the epithelial-to-mesenchymal transition, causing at least partial down-regulation of epithelial cell-specific molecules.[12] Considering the above possibility, we hypothesized that multivalent link of two distinct antibodies against a typical CTC to functionalized PAMAM dendrimers could significantly enhance the specificity of the conjugate to recognize and capture the wanted CTCs, and further result in down-regulation of the activity of the captured CTCs.

To test the hypothesis, we selected hepatocellular carcinoma HepG2 as a CTCs model as others have done,[13] and re-engineered PAMAM dendrimers with two antibodies to examine

J. Xie, Y. Lu, H. Dong, R. Zhao, H. Chen, W. Shen, Y. Zhu, J. Wang, Dr. J. Shao, Dr. Y. Gao, Prof. L. Jia
Cancer Metastasis Alert and Prevention Center
College of Chemistry
Fuzhou University
Fuzhou 350002, China
E-mail: pharmlink@gmail.com; shaojingwei@fzu.edu.cn
Prof. P. J. Sinko
Rutgers, The State University of New Jersey
160 Frelinghuysen Road, Piscataway, NJ 08854, USA
Dr. J. Shao, Prof. L. Jia
Biopharmaceutical Photocatalysis
State Key Laboratory of Photocatalysis on Energy and Environment
Fuzhou University
Fuzhou 350002, China
Dr. F. Xie
Department of Medicine Oncology
East Hospital of Xiamen University
Fuzhou 350004, China

DOI: 10.1002/adfm.201403556

the capture and regulation capabilities of the conjugates with this regard. The two antibodies are the human epithelial cell adhesion molecule (EpCAM) antibody (aEpCAM), and type II carbohydrate antigen saliva acidifying louis oligosaccharides X molecule (Sialyl Lewis X, Slex) antibody (aSlex). We selected HepG2 as a CTC model because liver cancer is one of the major threat cancers in China, and we have a good understanding of cellular characteristics of HepG2 cells.[14] The above-mentioned two biomarkers are over-expressed on HepG2. Spatial and temporal advances in high-payload and coating of PAMAM dendrimers allow us to explore the new initiative to capture and restrain CTCs in blood by using the dual antibody conjugation strategy. Yet, the quantitative and qualitative analyses of the interaction between the special conjugates and HepG2 have not been available, and the present studies with the conceptual advantage may provide the important information to the field.

2. Results

2.1. Physiochemical Characterization of Conjugates

Modified PAMAM dendrimer surfaces were sequentially functionalized with dual antibodies with or without fluorescence labeling (**Figure 1**A). The single or dual antibody conjugation was performed at the molar ratio of 1 CC G6 to 3 or 5 aSlex or aEpCAM. Thus we denoted the synthesized single conjugates as G6–3aEpCAM, G6–5aEpCAM, G6–3aSlex, and G6–5aSlex, or dual conjugates as G6–3aEpCAM-3aSlex and G6–5aEpCAM-3aSlex. Physiochemical characterization of the conjugates was conducted using spectral analyses, field scanning electron microscope (FSEM), and atomic force microscope (AFM), respectively. The conjugates were in a characteristic morphology of round pie with the 1 nm height. The diameter of the single antibody-coated dendrimers was approximately 35 ± 5 nm, and that of the dual antibody-coated dendrimers was 100 ± 5 nm (Figure 1B,D). Dynamic light scattering (DLS) measurements also demonstrated the increased hydrophilic size and negative charge once dendrimers were coated with aEpCAM or aSlex, separately, or in combination. The change in charge of the antibody-coated conjugates may influence their interaction with cells and blood components. Characteristic fluorescent colors and ultraviolet absorption values at $\lambda_{220\ nm}$ further demonstrated the successful conjugation of each

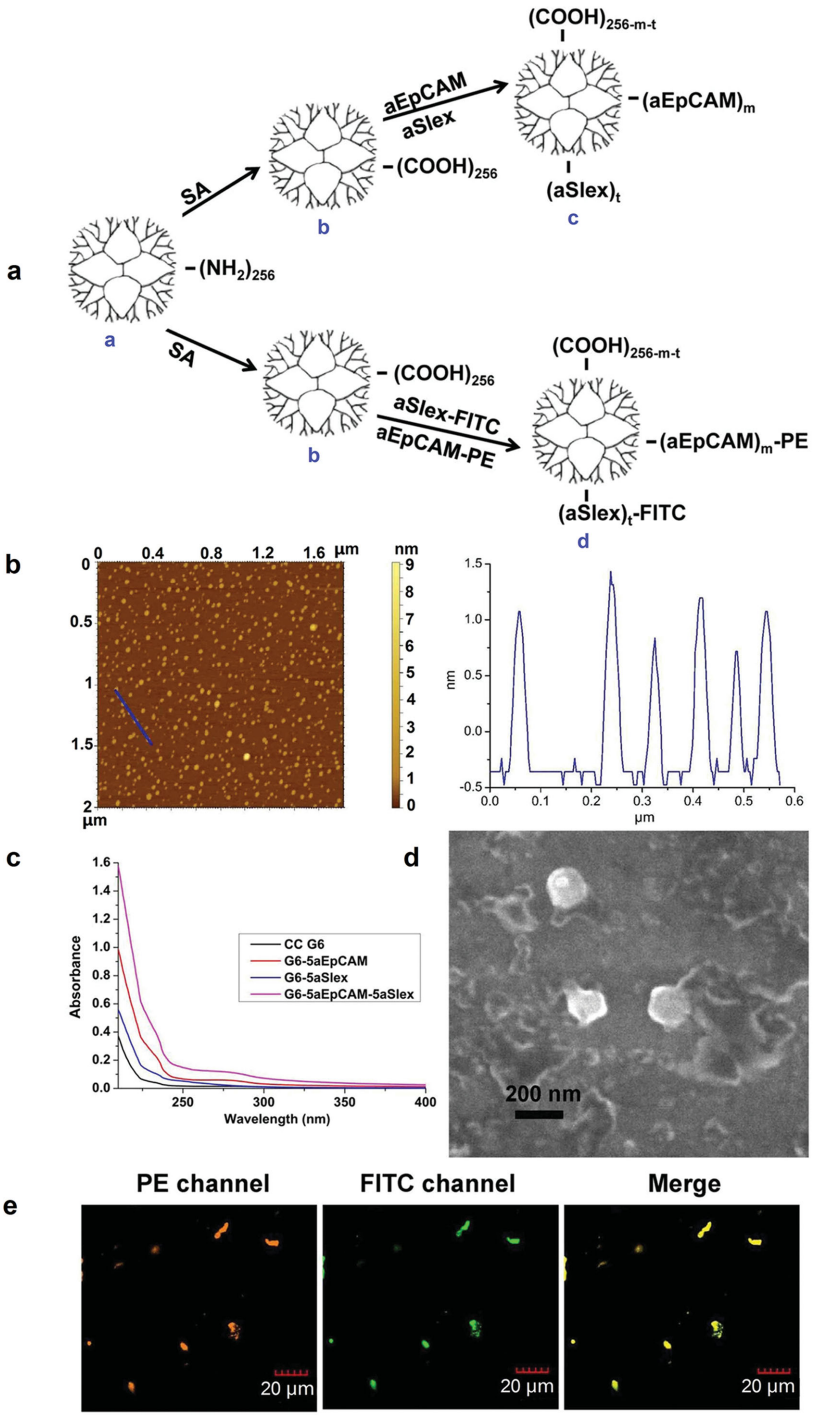

Figure 1. Conceptual design and characterization of surface functionalized G6 PAMAM dendrimers coated with single or dual antibodies of CTCs biomarkers (EpCAM and Slex) for the enhanced capture and down-regulation of target hepatocellular CTCs in blood. A) Synthetic procedures of G6 PAMAM dendrimers coated with single or dual antibodies with or without fluorescence labeling (PE and FITC). a) G6 PAMAM dendrimers with primary amine end groups; b) CC G6 dendrimers with carboxyl end groups; c) G6-single or dual antibody conjugates; d) fluorescence-labeled G6-single or dual antibody conjugates. B) A typical AFM image of single antibody conjugate G6–3aEpCAM. C) UV spectra of CC G6 and G6-single or dual antibody conjugates. D) A representative FSEM image of dual antibody conjugate G6–5aEpCAM-5aSlex. E) Fluorescence images of dual antibody conjugate PE-3aEpCAM-G6–3aSlex-FITC in PBS (pH 7.4) solution obtained by a laser confocal microscope in different excitation channels.

fluorescence-labeled antibody or antibody to dendrimer surfaces (Figure 1C,E). The amount of antibody in each single antibody conjugate was also calculated based on the corresponding linear curves of free aEpCAM and aSlex at $\lambda_{220\ nm}$. The UV spectra analysis showed that about 2 aEpCAM or 6 aSlex molecules were conjugated onto one G6 PAMAM dendrimer surface, respectively.

2.2. Microscopic and Flow Cytometric Analyses for HepG2 Recognition, Multivalent Binding, and Capture

To intuitively visualize the binding and capture efficiency of HepG2 cells in the absence or presence of interfering blood cells, fluorescein isothiocyanate (FITC, green fluorescence) was linked to aSlex (aSlex-FITC), and phycoerythrin (PE, orange fluorescence) to aEpCAM (aEpCAM-PE), respectively. The resultant products were then coated onto the dendrimer surface. The final fluorescence-labeled conjugates were denoted as G6–3aEpCAM-PE, G6–5aEpCAM-PE, G6–3aSlex-FITC, G6–5aSlex-FITC, PE-3aEpCAM-G6–3aSlex-FITC, and PE-5aEpCAM-G6–3aSlex-FITC, respectively. The number represents the estimated moles of the antibodies conjugated to the G6 PAMAM.

2.3. Binding and Capturing HepG2 Cells in the Absence of Interfering Blood Cells

For the adherent HepG2 cells, fluorescent images (**Figure 2**A) showed blue fluorescence in cell nuclei, indicating the integrity of HepG2. When HepG2 was exposed to fluorescence-labeled antibody or conjugates, the cells displayed the merged fluorescent colors. Orange color showed that the cells bound to aEpCAM-PE or G6–5aEpCAM-PE, and green color indicated the cells bound to aSlex-FITC or G6–3aSlex-FITC. The merged yellow-green color indicated that the cells bound to dual antibody conjugate PE-5aEpCAM-G6–3aSlex-FITC. Moreover, compared with the cells incubated with aSlex-FITC and aEpCAM-PE alone, stronger fluorescence on the cells treated with single or dual antibody-coated conjugates suggested a multivalent-mediated enhancement in binding affinity when dual antibody conjugates were bound to multiple surface biomarkers (Figure 2A).

For the suspensory HepG2 cells, the capture capability of the conjugates was evaluated in two ways when cells were at

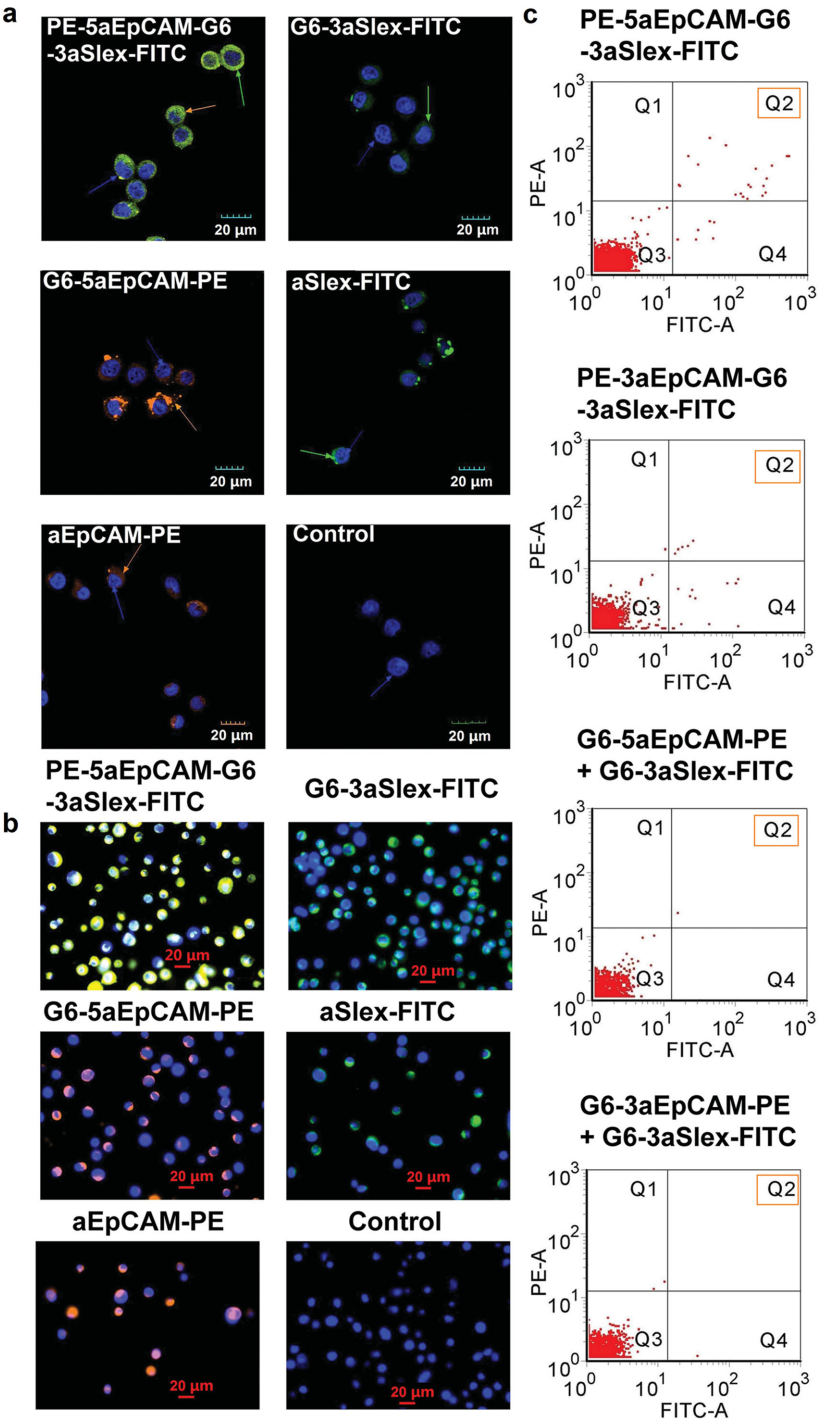

Figure 2. Microscopic and flow cytometric analyses of the bound or captured HepG2 cells by fluorescence-labeled single or dual antibody conjugates without any interference. Fluorescence-labeled antibodies including aEpCAM-PE and aSlex-FITC were also tested for the specific antigen–antibody interactions. A) Binding between the adherent HepG2 cells and conjugates imaged by a laser confocal microscope. B) Capturing the suspensory HepG2 cells by the conjugates imaged by a fluorescence inverted microscope. C) Dot plots showed the numbers of captured HepG2 cells within Q2 quadrant (i.e., cells positive to both FITC and PE dyes) by dual antibody conjugates PE-5aEpCAM-G6–3aSlex-FITC or PE-3aEpCAM-G6–3aSlex-FITC (right-upper two panels) or their single counterparts added together G6–5aEpCAM-PE+ G6–3aSlex-FITC or G6–3aEpCAM-PE+ G6–3aSlex-FITC (right-lower two panels). Dual antibody conjugate PE-5aEpCAM-G6–3aSlex-FITC captured HepG2 20-fold more than two single ones added together or 4-fold more than its counterpart PE-3aEpCAM-G6–3aSlex-FITC.

the density of 10^6 per incubation tube: 1. Fluorescent analysis: HepG2 was pretreated with Hoechst 33258 to show the presence of the cells, which were then incubated with fluorescence-labeled antibody or conjugates for 1 h. Compared with the control, cells treated with the antibody or conjugates displayed different colors on cytomembrane in addition to the blue color in nucleus. The result was indicative of the capture of the cells by the conjugates. Moreover, with the amounts of antibody aEpCAM or aSlex conjugated onto each dendrimer increased, more cells were captured by the conjugates in comparison with the fluorescence-labeled antibody aEpCAM-PE or aSlex-FITC alone. Dual antibody-coated dendrimers PE-5aEpCAM-G6–3aSlex-FITC seemed to capture more floating HepG2 cells than any single antibody-coated dendrimers G6–5aEpCAM-PE or G6–3aSlex-FITC alone or added together (Figure 2B). The enhancement in recognizing, binding and capturing HepG2 by the conjugates first confirmed our assumption that dendrimers conjugated with dual antibodies may be superior to those conjugated with the single ones in terms of capture efficiency.

2. Flow cytometric analysis: the floating HepG2 cells were incubated with the mixture of single antibody-coated dendrimers G6–3aEpCAM-PE plus G6–3aSlex-FITC, or G6–5aEpCAM-PE plus G6–3aSlex-FITC, or G6–5aEpCAM-PE plus G6–5aSlex-FITC, or individual dual antibody conjugates PE-3aEpCAM-G6–3aSlex-FITC and PE-5aEpCAM-G6–3aSlex-FITC at the final concentration of 20 μg mL^{-1} for 1 h. Flow cytometric analysis was performed to determine the capture efficiency of the conjugates on HepG2 cells after normalization of fluorescence intensity obtained from isotype controls IgG-PE and IgG-FITC. The numbers of HepG2 cells captured in Q2 plot quadrant by the dual antibody conjugates PE-3aEpCAM-G6–3aSlex-FITC or PE-5aEpCAM-G6–3aSlex-FITC were more than those captured by the single antibody conjugates added together (Figure 2C).

2.4. Capturing HepG2 Cells in the Presence of Interfering Blood Cells

The capture specificity, on the basis of our previous definition,[15] was defined as the ability to assess unequivocally the CTCs captured in the presence of components (red blood cells (RBCs), white blood cells (WBCs)) that may interrupt the quantitative measurement, while maintaining their own characteristics. The specificity of the conjugates binding to the surface of HepG2 cells was examined by mixing a series of HepG2 with either HL-60 cells (as a leukocyte model), or RBCs at a mixture ratio of $1:10^3$ or $1:10^5$ (HepG2: HL-60; or HepG2: RBCs) with fixed total 10^6 cells per incubation tube, or by mixing 1000 HepG2 cells with 10^6 or 10^8 RBCs per incubation tube. HL-60 cells usually have no interaction with aEpCAM.[16] The ratio mimicked the clinical situation in which, roughly 1 CTC presented in 10^3–10^6 leukocytes,[17] or 100 CTCs in 10^8 RBCs.[18] Sample analysis and data collection were performed after 1 h incubation of the HepG2 with the fluorescence-labeled conjugates.

The gate conditions for HepG2 cells were set to compensate for FITC and PE dyes followed by dot plotting to show the numbers of HepG2 cells captured by the conjugates. In general, the conjugates recognized and bound HepG2 in a cooperative manner in the presence of either HL-60 or RBCs, whereas, the isotype IgG control did not bind or capture the suspended HepG2 cells.

PE-5aEpCAM-G6–3aSlex-FITC conjugate captured more HepG2 cells than PE-3aEpCAM-G6–3aSlex-FITC conjugate in the presence of abundant interfering RBCs (**Figure 3**A,D). Capture efficiency of PE-5aEpCAM-G6–3aSlex-FITC and PE-3aEpCAM-G6–3aSlex-FITC was 30.9% and 10.7%, respectively (Figure 3A), at the number ratio of HepG2:RBCs in $1:10^3$, suggesting the important role of aEpCAM in capturing HepG2. The percentage of bound and captured HepG2 by those conjugates decreased when the mixed cell ratio of HepG2 to HL-60 or RBCs changed from $1:10^3$ to $1:10^5$ (HL-60), or from 10^6 to 10^8 (RBCs) (Figure 3A–D), probably due to the interference from RBC or HL-60. The capture efficiency or captured cell number of dual antibody conjugates (e.g., PE-5aEpCAM-G6–3aSlex-FITC) was 3- to 15-fold higher in the presence of interfering cells, especially RBCs, in comparison with that of single antibody conjugates G6–5aEpCAM-PE and G6–5aSlex-FITC (Figure 3B,C). Similarly, a reduction in the number of the captured HepG2 was observed when the number of interfering RBCs was increased (Figure 3D).

2.5. Regulation by the Conjugates on Viability of Captured HepG2 Cells

In comparison to the control completely carboxylated G6 (CC G6) dendrimers and its single antibody counterparts, the G6–5aEpCAM-3aSlex conjugate produced a significant reduction in cell viability when the conjugate concentrations increased from 5, 10 to 20 μg mL^{-1} (**Figure 4**A). In contrast, CC G6, G6–3aSlex, and G6–5aEpCAM at molar concentrations of 3- to 5-fold higher than G6–5aEpCAM-3aSlex did not have the significant effect (Figure 4A). To further determine how these conjugates affected the viability of the captured cells, cell cycle distribution was analyzed by flow cytometry using the propidium iodide (PI) staining to reveal the percentage of HepG2 arrested by the conjugates in the phases of G0/G1, S, and G2/M, respectively, after 24- and 48-h binding treatment. The CC G6 was used as a control. The results indicated that G6–5aEpCAM, G6–3aSlex, and G6–5aEpCAM-3aSlex produced a concentration-dependent increase in cell population of the S-phase and a reduction in the G2/M phase cell population without a significant effect on the G0/G1 phase cell population (Figure 4B,C). We, therefore, concluded that the conjugates could deactivate the captured CTCs by arresting the cells in the DNA synthesis S phase and preventing them from going into the G2/M checkpoint.

2.6. Cell Apoptosis Analysis

The conjugates seemed to produce somewhat early apoptosis or necrosis on the captured HepG2 cells. G6–5aEpCAM-3aSlex conjugate (20 μg mL^{-1}) resulted in approximately 40% increase in early apoptotic cell population without a significant effect on necrotic cell population in comparison with the control. When the concentrations of G6–5aEpCAM and G6–3aSlex conjugates

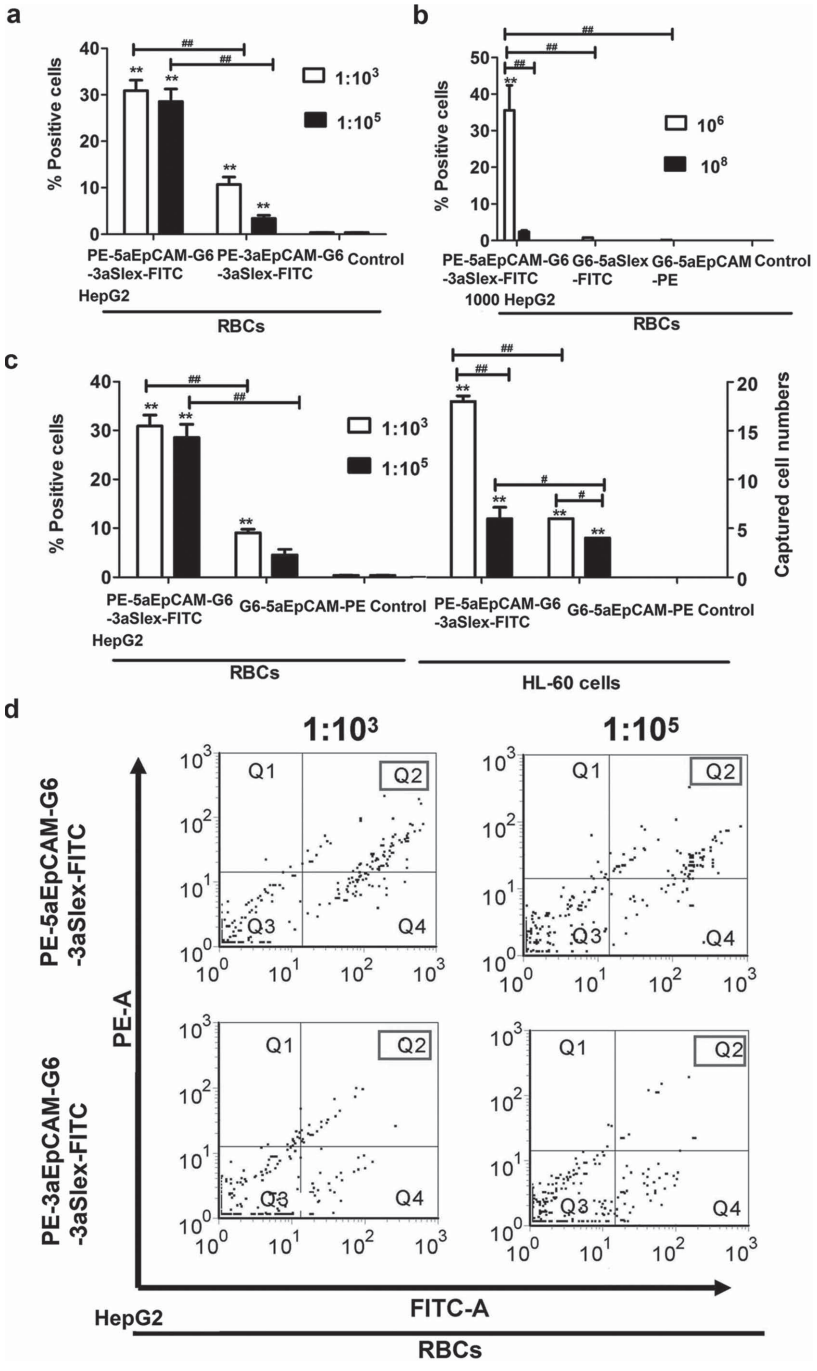

Figure 3. Capture efficiency of fluorescence-labeled single or dual antibody conjugates at capturing HepG2 cells in the presence of interfering RBCs or HL-60 cells. The capture efficiency was determined either by% positive cells or by the captured cell numbers. A) PE-5aEpCAM-G6–3aSlex-FITC conjugate showed the enhanced capture efficiency for HepG2 as compared to its counterpart PE-3aEpCAM-G6–3aSlex-FITC when HepG2 was mixed with the interfering cells RBC at the number ratio of $1:10^3$ and $1:10^5$. B) Comparison of the capture efficiency between dual antibody conjugate PE-5aEpCAM-G6–3aSlex-FITC and single antibody conjugates (G6–5aEpCAM-PE and G6–5aSlex-FITC) when 1000 HepG2 cells were spiked into 10^6 or 10^8 RBCs. C) Dual antibody conjugate PE-5aEpCAM-G6–3aSlex-FITC exhibited the higher capture efficiency than single antibody conjugate G6–5aEpCAM-PE when the number ratios of HepG2: RBC or HL-60 were in $1:10^3$ and $1:10^5$. D) Flow cytometric images of the captured $FITC^+PE^+$ HepG2 cells in Q2 plot quadrant by dual antibody conjugates PE-5aEpCAM-G6–3aSlex-FITC and PE-3aEpCAM-G6–3aSlex-FITC. Note, the former captured more HepG2 (Q2 plot of the upper two panels) than the latter (Q2 plot of the lower two panels).

reached 20 μg mL^{-1}, G6–5aEpCAM and G6–3aSlex conjugates caused no significant increase in apoptotic cell population but about 20% increase in necrotic cell population (**Figure 5**A). Decrease in cellular mitochondrial membrane potential (MMP) induced by single or dual antibody conjugates also reflected the moderate regulation on cell activity, which was in agreement with the above cytotoxic and cell apoptotic analyses (Figure 5B).

2.7. CTCs Captured in Blood of Liver Cancer Patients

The capture efficiency of the single or dual antibody conjugates was determined based on the positive numbers shown in the plot quadrant of the flow cytometer. Distinguished from WBCs, the CTCs from patient blood were characterized by three-color immunocytochemistry (dihydrochloride (DAPI), FITC anti-cytokeratin, PE anti-CD45) as described in recent CTC detection and capture studies.[8,19] Only cells that were $DAPI^+CD45^-$cytokeratin$^+$ with the appropriate size and morphology were identified as CTCs. PE^+APC^--labeled and $FITC^+APC^-$-labeled cells were determined, respectively, as the CTCs captured by the single antibody conjugate G6–5aEpCAM-PE and G6–5aSlex-FITC, while $PE^+FITC^+APC^-$-labeled cells were determined as the CTCs captured by the dual antibody conjugate PE-5aEpCAM-G6–3aSlex-FITC (**Figure 6**A). In 50 000 cells collected by the flow cytometer, the average number of CTCs captured by the dual antibody conjugate was 4 ± 4 mL^{-1} blood of liver cancer patients ($n = 7$), whereas, the single antibody conjugate G6–5aSlex-FITC captured 2 ± 2 CTCs, and G6–5aEpCAM-PE captured fewer CTCs per mL blood of liver cancer patients ($n = 7$) under the same conditions (Figure 6B). The result was consistent with what was shown in Figure 3, and strongly suggests that the dual antibody conjugate is superior to its single counterparts in capturing CTCs.

3. Discussion

In the present study, we made use of the spatial and high payload advances of PAMAM dendrimer nanomaterials to sequentially coat two antibodies of CTCs surface biomarkers (aEpCAM and aSlex) onto the surface functionalized nanomaterials. The conjugation

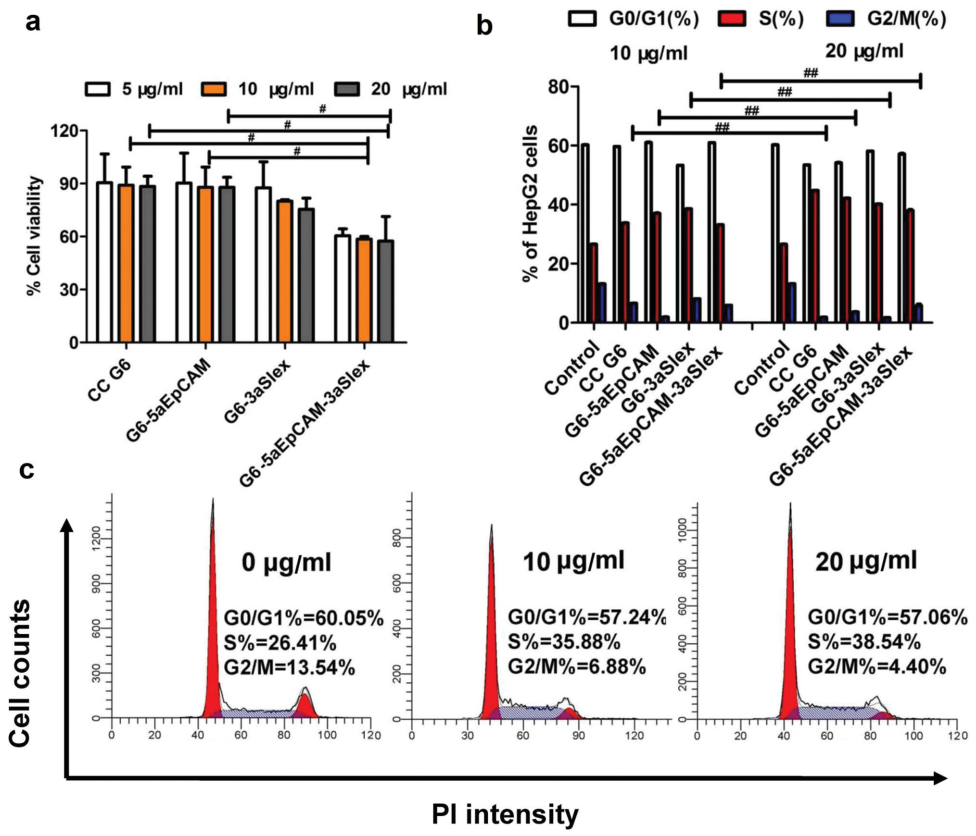

Figure 4. Cell viability and cell cycle distribution of HepG2 when incubated with the conjugates (10 and 20 μg mL^{-1}). A) Changes in cell viability of the captured HepG2. The dual antibody conjugate G6–5aEpCAM-3aSlex inhibited HepG2 viability more potently. B) Distribution of HepG2 cell population in G0/G1, S, and G2/M phases. In comparison with the control, single or dual antibody conjugates caused an increase in cell population of the S phase and a decrease in that of the G2/M phase. C) DNA flow cytometric images of HepG2 cells captured by the dual antibody conjugate G6–5aEpCAM-3aSlex. Compared with the control, cell population in S phase was concentration-dependently increased after capturing.

technology seems to be practically applicable to creating dual antibody coated conjugates with the enhanced specificity and capacity to bind and capture CTCs. The synthesis was successful and documented by the physiochemical characterization using FSEM, AFM, DLS, fluorescent imaging, and other sophisticated means to demonstrate each molecular entity. The

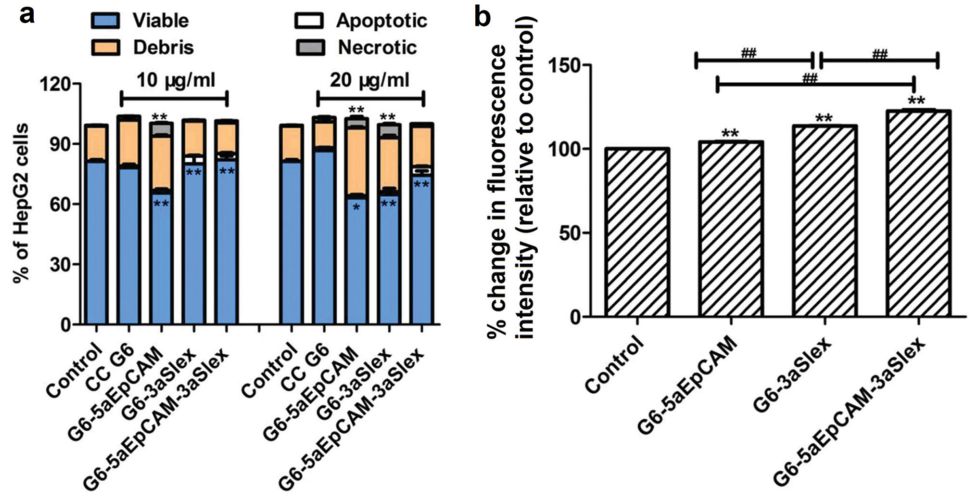

Figure 5. Flow cytometric analysis of cell apoptotic status and cellular MMP induced by single or dual antibody conjugates. A) Annexin V-FITC/PI apoptotic analysis. B) Changes in cellular MMP induced by the conjugates at the same concentration of 10 μg mL^{-1}. Compared to the control, the increased fluorescence intensity of DiOC6(3) usually indicates the decreased cellular MMP. The dual antibody conjugate produced more descent in MMP.

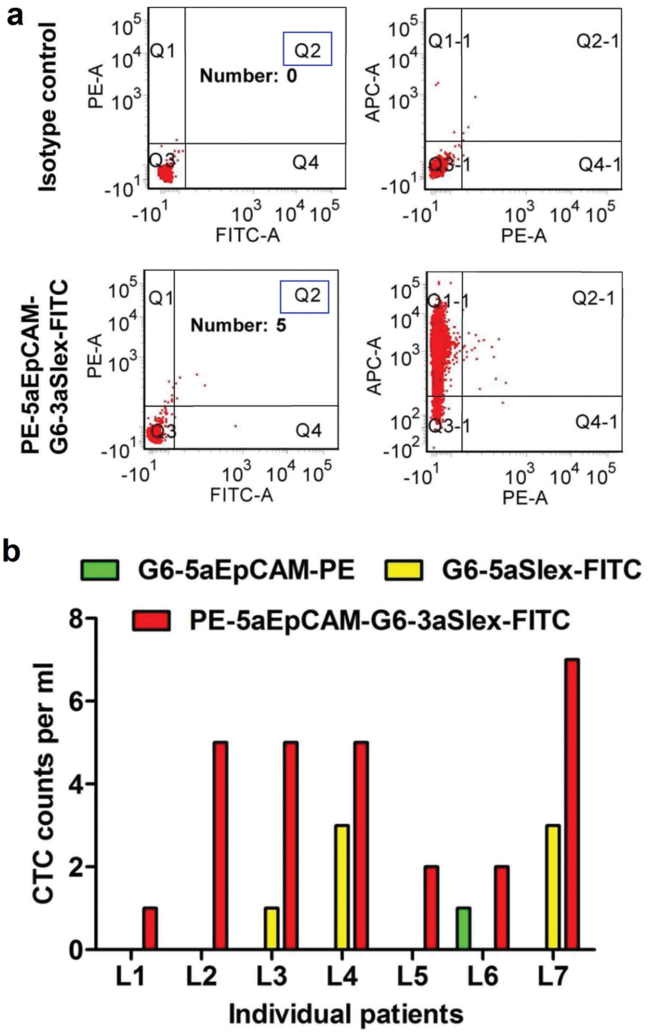

Figure 6. Analysis by flow cytometry of CTCs captured from 1 mL blood of liver cancer patients at mid-to-late stage. A) Representative images of captured CTCs from a patient blood by dual antibody conjugate PE-5aEpCAM-G6–3aSlex-FITC in comparison with the isotype control. The number shown in the Q2 plot quadrant indicates the number of CTCs captured. B) Numbers of CTCs captured by the single or dual antibody conjugates from seven patients' blood. Dual antibody conjugate PE-5aEpCAM-G6–3aSlex-FITC captured more CTCs than its single counterparts (G6–5aEpCAM-PE and G6–5aSlex-FITC).

fluorescence-labeled or nonfluorescence labeled antibody–dendrimer conjugates seemed to be biostable under various conditions. We tested their binding and capture effects on HepG2 cells in the presence and absence of abundant interfering blood cells, i.e., HL-60 cells and RBCs, and on CTCs in liver cancer patients. We further demonstrated whether the capture could result in down-regulation of HepG2, and elucidated the related mechanisms of actions. The novelty of the present study lies in that we, for the first time, created the dual antibody-coated nanomaterial conjugates to specifically capture and restrain CTCs in blood of liver cancer patients. To the best of our knowledge, it is the first time that this conceptual advance was practically tested. The initiative could guide us to design a more specific and efficient nano-conjugate to restrain the residual CTCs in patient blood.

Dendrimers have the high-branched nanoscale structure with large numbers of the functional groups, which possess the superior properties such as biocompatibility, biodegradability, biosafety as well as the mediated multivalent binding effect.[7,20] Therefore, dendirmers as promising candidates of carriers were widely used for cancer treatment, especially for targeted drug delivery.[21] Different from the reported conjugation methods using heterobifunctional cross-linkers,[22] we took the 1-ethyl-3-(3-dimethylaminopropyl) carbodiimide (EDC) and N-hydroxy-succinimide (NHS) catalytic method[7] for surface functionalization of the dendrimers to sequentially conjugate the aEpCAM and aSlex antibodies onto the functionalized dendrimers for the first time (Figure 1). The re-engineering process seemed to be successful, and the two antibodies could be spatiotemporally accommodated.

Given the fact that the transmembrane glycoprotein EpCAM is expressed on the surface of a wide variety of solid-tumor cells but not of the normal cells found in blood,[23] and Slex is frequently expressed on tumor cell lines and closely correlated with the process of cancer metastasis,[17,24] stationary binding and capture studies in vitro clearly displayed that the single or dual antibody conjugates could specifically bind to the EpCAM and Slex-expressing HepG2 cells (Figure 2). The strong fluorescence from the bound cell surface might be attributed to the dendrimer-mediated multivalent binding effects by multiple antigen-antibody interactions[7,20b] and the enhanced local topographic interactions between antibody-coated dendrimers and various components on the cell surface.[9a,b,25] The maximum capture efficiency by PE-5aEpCAM-G6–3aSlex-FITC conjugate was 30.8% or 35.6% (Figure 3A–C), when the mixture ratio of HepG2:RBCs was $1{:}10^3$, or 1000 HepG2 cells were spiked into 10^6 RBCs. The dual antibody conjugate PE-5aEpCAM-G6–3aSlex-FITC also exhibited higher binding and capture capacity than the single antibody conjugates (Figure 3B,C). The enhanced capture efficiency might be due to the double specificity and selectivity of the conjugates toward two tumor cell surface biomarkers.

The dual antibody conjugate G6–5aEpCAM-3aSlex (20 μg mL^{-1}) showed the 42% antiproliferation ability (Figure 4A). The down-regulation on HepG2 cells might be ascribed to the direct effect of the dendrimers on the captured cells,[26] antibody–antigen interactions,[27] and endocytosis role of cells themselves.[28] Interestingly, when the concentration unit of these conjugates was converted to the molar concentration (nM), G6–5aEpCAM-3aSlex, G6–3aSlex, and G6–5aEpCAM at 20 μg mL^{-1}, respectively, exhibited the mean growth inhibition rate of 26.6% ± 15.1%, 11.2% ± 5.0%, and 2.3% ± 1.9% on the HepG2 cells based on the effect of the CC G6 used as the control (0.4% ± 0.4%). Cell cycle distribution and cell apoptosis analyses demonstrated the conjugates could arrest the captured cells in S phase and result in a decrease in cell population going into the G2/M phase (Figure 4B,C). Consequently, cells were induced into early apoptotic stage. Cellular MMP measurement and morphological evaluation were in agreement with above results (Figure 5, Figure 1, Supporting Information). The potent inhibition by the dual antibody conjugate against the captured HepG2 provides additional evidence of the enhanced

capture specificity of the dual antibody conjugate because specific capture usually produces greater inhibition.

CTCs-capture study of patient samples is indicative of the clinical applicability of the dual antibody-conjugation technology. In comparison with the reported studies in which only ≤7 CTCs per 7.5 mL of breast cancer patient blood were detected by microfluidic approaches and CellSearch platform,[29] or average 3–5 CTCs per mL blood of breast, pancreatic, lung cancer patients were captured by using functionalized graphene oxide nanosheets on a patterned gold surface,[8] our novel strategy not only has a significant advantage in specifically capturing more CTCs (Figure 6), but also shows the great potential in capturing and down-regulating CTCs in vivo.

In summary, the present study applied a novel nanotechnology strategy to the advanced conception of capturing and restraining CTCs in blood. The spatially-branched and high payload dendrimers were used to accommodate dual antibodies against two distinct biomarkers of CTCs to enhance the specificity of capturing and restraining patient CTCs and HepG2 in the presence and absence of abundant interfering blood cells. As the result of re-engineering, the dual antibody conjugates showed improved multivalent capturing and restraining effects on the CTCs. The study provides a new conception to design more effective nanomedicines for capturing and restraining CTCs in patient blood.

4. Experimental Section

Synthesis of G6 PAMAM Dendrimer–Antibody Conjugates: G6 PAMAM dendrimers (62 400 Da) with primary amine end groups of 256 were chosen as the scaffolds to assemble aEpCAM and/or aSlex following complete carboxylation of the G6 dendrimers. Dendrimers G6 reacted with succinic anhydride (SA) to form the CC G6 and partially carboxylated G6 PAMAM (PC G6) dendrimers. PC G6 dendrimers were covalently reacted with FITC at pH 9.5, then with antibodies at pH 7.4. The conjugation reaction was carried out using EDC/NHS conjugation chemistry. CC G6 dendrimers, once activated by EDC and NHS, directly reacted with aEpCAM and aSlex (aEpCAM-PE and aSlex-FITC) for synthesis of the conjugates. Purified human aEpCAM (MW150 KDa) were provided by Abcam (Hong Kong) Ltd. Human aSlex (MW150 KDa), aSlex-FITC, and aEpCAM-PE were purchased from BD company. All the derivatives and conjugates were purified via dialysis (10 000 MWCO) against deionized water and followed by lyophilization.

Characterization Procedures of the Conjugates: Chemical structures of all dendrimer derivatives and conjugates were confirmed by spectral analyses including ^{1}H NMR (an AVANCE III 500 MHz NMR system, Bruker, Switzerland) in D_2O and FTIR (a Nicolet 360 Fourier Transform IR spectrometer, Nicolet Instruments, Inc.). Distribution of zeta potential (mV) and hydrodynamic diameter (nm) was measured by a Zeta potential/dynamic light scattering analyzer (Zetaplus/90plus, BIC, Brookharen). Surface morphology and particle size were determined by FSEM (Nova NanoSEM 230) and AFM (Agilent AFM 500, tapping probe 40 N m^{-1}, in AC mode) images. The numbers of FITC molecules in each PC G6 dendrimers and antibody in each single antibody conjugate were respectively calculated according to the corresponding fluorescence intensity at λ_{ex} 492 nm, λ_{em} 530 nm, and UV absorption value at $\lambda_{220\ nm}$. Fluorescence-labeled antibody conjugated on dendrimer surface was further demonstrated by using a laser confocal microscope (Olympus FluoView 1000), respectively, at FITC λ_{ex} 488 nm, λ_{em} 500–535 nm and PE λ_{ex} 543 nm, λ_{em} 560–660 nm. The stability of the conjugates was measured under static or dynamic conditions at different pHs (5.6, 7.4, 9.13), T °C (4, 37 °C), vibration rates (80, 120, 210 rpm) and incubation intervals. Changes were determined by UV spectral analysis.

Cell Culture: Human HepG2 and HL-60 leukemia cells were cultured in RPMI 1640 medium supplemented with 10% heat-inactivated fetal calf serum (FCS) and 1% penicillin/ streptomycin (P/S) in a humidified atmosphere of 5% CO_2 at 37 °C. HepG2 cells at final density of 10^5–10^6 cells per mL were grown in 96-well plates for MTT {[3-(4,5-dimethylthiazol-2-yl)-2,5-diphenyltetrasodium bromide] tetrazolium salt} assay, 6-well plates for flow cytometric analysis, and 35 mm dishes with glass coverslips on the bottom for confocal microscopic observation. RBCs were obtained from the fresh blood after centrifugation.

Flow Cytometry Procedures: Flow cytometric analysis was performed on a Becton Dickinson (BD) multiparametric fluorescence-activated cell sorting (FACS) Aria III cell sorter with laser excitation set at 488 and 633 nm. Fluorescence signals derived from PI or PE were detected through 585 nm bandpass filters. Fluorescence signals derived from iodide [3,3′-dihexyloxacarbocyanine iodide] (DiOC6(3)) or FITC were detected through 530 nm bandpass filters. Fluorescence signals derived from APC were detected through 660 nm bandpass filters. Data acquisition was collected based on 10 000 or 50 000 cells satisfying the light scatter criteria. Initial data analysis was performed using the BD FACS Diva software. The antibodies used in the capture assay were aEpCAM-PE and aSlex-FITC, which were pre-conjugated onto dendrimer surfaces by covalent-coupling reactions. Immunoglobulins labeled with the same fluorochromes IgG-PE, IgG-FITC and IgG-APC were used as isotype controls to exclude the autofluorescence and nonspecific binding. Gating strategy focused on identifying and quantifying the conjugate-captured FITC$^+$PE$^+$ HepG2 cells from the large populations of HL-60 cells or RBCs, or the whole blood of patients. We set P1 gate as the total target HepG2 cells according to the forward versus side scatter histograms. Compensation was made for FITC and PE dyes followed by dot plots to show the number of fluorescence-labeled conjugates bound to HepG2 cells. Each plot quadrant showed the number of aSlex-bound cells (FITC channel) versus aEpCAM-bound ones (PE channel). The average number of the conjugate-captured FITC$^+$PE$^+$ HepG2 cells was shown within Q2 plot quadrant.

Cell Binding and Capture Assays: To investigate binding interaction between single or dual antibody conjugates and the adherent HepG2 cells, laser confocal microscopic analysis was performed. Cells at a density of 10^5 per mL evenly were seeded on 35 mm dishes with glass coverslips on the bottom and incubated with serum-free medium containing fluorescence-labeled antibodies (aEpCAM-PE and aSlex-FITC) or conjugates (G6-aEpCAM-PE, G6-aSlex-FITC, and PE-aEpCAM-G6-aSlex-FITC) at the same concentration of 20 μg mL^{-1} at 37 °C in a humidified atmosphere of 5% CO_2 for 1 h after pretreatment with phosphate-buffered saline (PBS) containing 1% bovine serum albumin (BSA) (1% PBSA) for 30 min. Cells were washed and fixed with stationary liquid ($V_{methanol}$:$V_{acetone}$ = 7:3) for 1 min, and stained with PBS buffer containing the nuclei stain DAPI (10 μg mL^{-1}, blue color) for 15 min. Finally, cells were rinsed and covered with serum-free medium for analysis by using an Olympus FluoView 1000 laser scanning confocal microscope, respectively, at FITC λ_{ex} 488 nm, λ_{em} 500–535 nm, and PE λ_{ex} 543 nm, λ_{em} 560–660 nm. To investigate capture capability of the single or dual antibody conjugates, the floating HepG2 cells were treated in two ways: (1) 10^6 cells in each tube were first stained with Hoechst 33258 (blue color) for 15 min to confirm the presence of cell nucleus, cells were then mixed with PBS containing fluorescence-labeled antibodies (aEpCAM-PE and aSlex-FITC) and conjugates (G6-aEpCAM-PE, G6-aSlex-FITC, and PE-aEpCAM-G6-aSlex-FITC), separately, for 1 h at 37 °C water bath in dark after pretreatment with 1% PBSA for 30 min. After removal of the unbound conjugates, cells were suspended in 100 μL PBS for imaging by a fluorescence inverted microscope (Axio Observer A1, Zeiss, Germany) at λ_{ex} 470/40 nm, λ_{em} 525/50 nm. (2) 10^6 cells in each tube were directly co-incubated with fluorescence-labeled dual antibody conjugates (PE-3aEpCAM-G6–3aSlex-FITC and PE-5aEpCAM-G6–3aSlex-FITC) or mixed with the single counterparts (G6–3aEpCAM-PE and G6–3aSlex-FITC, G6–5aEpCAM-PE and G6–3aSlex-FITC, G6–5aEpCAM-PE and G6–5aSlex-FITC) at final concentration of 20 μg mL^{-1} for 1 h at 37 °C water bath in dark after

pretreatment with 1% PBSA for 30 min and quantified on a BD FACS Aria III analyzer with laser excitation set at 488 nm. To quantitatively evaluate the cell capture efficiency of the conjugates toward HepG2 in the presence of numerous interfering cells, HepG2 was spiked with HL-60 cells and RBCs at number ratios of $1:10^3$ or $1:10^5$. Cell mixtures were treated with 1% PBSA to exclude the nonspecific binding and then individually incubated with 20 μg mL^{-1} fluorescence-labeled dual antibody conjugates (PE-3aEpCAM-G6–3aSlex-FITC and PE-5aEpCAM-G6–3aSlex-FITC) for 1 h at 37 °C water bath. After cells were washed with PBS for three times, flow cytometric analysis was performed based on the normalization of the fluorescence intensity using IgG-PE and IgG-FITC isotypes. The capture efficiency (% positive cells) was defined as the number of the conjugate-captured $FITC^+PE^+$ HepG2 cells in Q2 plot quadrant divided by the number of the cells shown in the P1 gate.

Cell Activity Regulation: The following assays were conducted to study HepG2 activity regulation by the single or dual antibody conjugates without fluorescent labeling (G6–5aEpCAM, G6–3aSlex, and G6–5aEpCAM-3aSlex).

Anti-proliferation Assay: Cell toxicity induced by the conjugates was tested by MTT assay. HepG2 cells were grew in 96-well plates in the confluence of 70%–80% and exposed to individual conjugate at various concentrations (0, 5, 10, 20 μg mL^{-1}) for 48 h. 100 μL serum-free medium containing 1 mg mL^{-1} MTT solution was added to each well. After incubation for another 4 h, the supernatant was aspirated and 150 μL DMSO was added to dissolve the water-insoluble blue formazan. The optical density of each well was read on an ELISA reader (Tecan Infinite M200 pro) at a wavelength of 570 nm and the survival rate was calculated by the absorption values of $A_{570\ nm}$ in the treated group compared to those in the control group.

Cell Cycle Analysis: The analysis procedure was similar to what we described before for evaluation on the effects of drugs on the distribution of cell population in every phase (G0/G1, S, and G2/M).[30] Briefly, HepG2 cells were incubated in 6-well plates. After treatment with various concentrations of conjugates (0, 10, 20 μg mL^{-1}) for 48 h, cells were trypsinized and washed with ice-cold PBS for three times. Cells were then collected and fixed with 70% ice ethanol overnight at –20 °C. Fixed cells were washed and stained with PI solution at 37 °C for 15 min in dark. Data acquisition and analysis was finally read on a flow cytometer (BD FACS Aria III). The side angle scattered light (SSC) versus PI histogram was shown for cell cycle analysis.

Cell Apoptosis Detection: Annexin V-FITC/PI apoptosis detection kit was used to quantitatively determine the apoptotic status of HepG2 cells after treatment. Cells were first cultivated on the 6-well plates and incubated with the conjugates (0, 10, 20 μg mL^{-1}) for 48 h followed by three times of washing with PBS, and harvested by centrifugation. 5 μL Annexin V-FITC, 5 μL PI, and 500 μL binding buffer were mixed and added to each tube for 15 min in dark. Cells at different stages were analyzed within 1 h by flow cytometric analysis. Briefly, FITC and PI fluorescent intensity and the percentage of cell population within each plot quadrant of dot plots represented distribution of cells in every stage (debris, viable, apoptotic and necrotic). Besides, SSC versus DiOC6(3) histogram was also displayed for MMP analysis.

MMP Measurement: Changes in MMP in HepG2 cells were evaluated by the method validated by us.[31] The assay was based on quantitative fluorescent analysis of DiOC6(3) in mitochondria following cell apoptosis. After incubation with the conjugates (0, 10, 20 μg mL^{-1}) for 48 h, cells were trypsinized and collected after centrifugation. Each tube was stained with 500 μL of 2×10^{-9} M DiOC6(3) working solution at 37 °C for 20 min. All the stained cells were examined by flow cytometry (BD FACS Aria III).

Quantification of Captured CTCs From Liver Cancer Patient Samples: Blood samples obtained from seven liver cancer patients at mid-to-late stage were collected into EDTA-containing vacutainer tubes according to the standard protocol approved by the institutional review board, and processed within 24 h. Fluorescence labeled-single or dual antibody conjugates (40 μg, 1 mL) were individually spiked into 1 mL of patient blood that was pretreated with 1% PBSA for 30 min. After 1 h incubation at 37 °C, the captured CTCs and WBCs were isolated from the lysed RBCs via centrifugation and blocked with 1% PBSA at room temperature for 30 min. The APC-conjugated anti-CD45 was added to label the WBCs at 37 °C for 30 min to exclude hematopoietic cells. Finally, all the residual cells were directly suspended in 500 μL PBS for quantitative analysis of the capture efficiency of the conjugates by using the flow cytometry. The quantitation was conducted following normalization for different fluorescent dyes (PE, FITC, and APC). Various kinds of isotypes were used as the controls to exclude the nonspecific binding and autofluorescence of cells.

Statistical Analysis: Data were presented as the means ± standard deviations of $n \geq 3$. Statistical analysis was done by Student's *t*-test and one-way analysis of variance by using the least significance difference (LSD) test (IBM SPSS Statistics 19.0). The symbol * and ** represented the comparison between sample and control, and # and ## represented the comparison between any two samples. A probability value of <0.05 was considered statistically different (* and #), and <0.01, statistically significantly different (** and ##).

Supporting Information

Supporting Information is available from the Wiley Online Library or from the author.

Acknowledgements

This work was supported by grants from the Ministry of Science and Technology of China (Grant No. 2015CB931804), National Science Foundation of China (Grant Nos. 81273548, 81201709, and 81472767), and National Institutes of Health (Grant No. 5R01 CA155061).

Received: October 11, 2014
Revised: November 30, 2014
Published online: January 21, 2015

[1] J. S. de Moor, A. B. Mariotto, C. Parry, C. M. Alfano, L. Padgett, E. E. Kent, L. Forsythe, S. Scoppa, M. Hachey, J. H. Rowland, *Cancer Epidemiol., Biomarkers Prev.* **2013**, *22*, 561.
[2] S. P. Leong, W. W. Tseng, *Ca-Cancer J. Clin.* **2014**, *64*, 195.
[3] S. L. Stott, R. J. Lee, S. Nagrath, M. Yu, D. T. Miyamoto, L. Ulkus, E. J. Inserra, M. Ulman, S. Springer, Z. Nakamura, A. L. Moore, D. I. Tsukrov, M. E. Kempner, D. M. Dahl, C. L. Wu, A. J. Iafrate, M. R. Smith, R. G. Tompkins, L. V. Sequist, M. Toner, D. A. Haber, S. Maheswaran, *Sci. Transl. Med.* **2010**, *2*, 25ra23.
[4] G. J. Rustin, M. E. van der Burg, C. L. Griffin, D. Guthrie, A. Lamont, G. C. Jayson, G. Kristensen, C. Mediola, C. Coens, W. Qian, M. K. Parmar, A. M. Swart, *Lancet* **2010**, *376*, 1155.
[5] L. G. Daenen, J. M. Roodhart, M. van Amersfoort, M. Dehnad, W. Roessingh, L. H. Ulfman, P. W. Derksen, E. E. Voest, *Cancer Res.* **2011**, *71*, 6976.
[6] S. Wang, H. Wang, J. Jiao, K. J. Chen, G. E. Owens, K. Kamei, J. Sun, D. J. Sherman, C. P. Behrenbruch, H. Wu, H. R. Tseng, *Angew. Chem. Int. Ed.* **2009**, *48*, 8970.
[7] J. H. Myung, K. A. Gajjar, J. Saric, D. T. Eddington, S. Hong, *Angew. Chem. Int. Ed.* **2011**, *50*, 11769.
[8] H. J. Yoon, T. H. Kim, Z. Zhang, E. Azizi, T. M. Pham, C. Paoletti, J. Lin, N. Ramnath, M. S. Wicha, D. F. Hayes, D. M. Simeone, S. Nagrath, *Nat. Nanotechnol.* **2013**, *8*, 881.
[9] a) K. E. Fischer, B. J. Aleman, S. L. Tao, R. Hugh Daniels, E. M. Li, M. D. Bunger, G. Nagaraj, P. Singh, A. Zettl, T. A. Desai, *Nano Lett.* **2009**, *9*, 716; b) S. K. Lee, G. S. Kim, Y. Wu, D. J. Kim, Y. Lu, M. Kwak, L. Han, J. H. Hyung, J. K. Seol, C. Sander, A. Gonzalez, J. Li, R. Fan, *Nano Lett.* **2012**, *12*, 2697; c) W. Chen, S. Weng,

F. Zhang, S. Allen, X. Li, L. Bao, R. H. Lam, J. A. Macoska, S. D. Merajver, J. Fu, *ACS Nano* **2013**, *7*, 566.

[10] I. Baccelli, A. Schneeweiss, S. Riethdorf, A. Stenzinger, A. Schillert, V. Vogel, C. Klein, M. Saini, T. Bauerle, M. Wallwiener, T. Holland-Letz, T. Hofner, M. Sprick, M. Scharpff, F. Marme, H. P. Sinn, K. Pantel, W. Weichert, A. Trumpp, *Nat. Biotechnol.* **2013**, *31*, 539.

[11] X. Ni, M. Zhuo, Z. Su, J. Duan, Y. Gao, Z. Wang, C. Zong, H. Bai, A. R. Chapman, J. Zhao, L. Xu, T. An, Q. Ma, Y. Wang, M. Wu, Y. Sun, S. Wang, Z. Li, X. Yang, J. Yong, X. D. Su, Y. Lu, F. Bai, X. S. Xie, J. Wang, *Proc. Natl. Acad. Sci. U.S.A.* **2013**, *110*, 21083.

[12] M. Yu, A. Bardia, B. S. Wittner, S. L. Stott, M. E. Smas, D. T. Ting, S. J. Isakoff, J. C. Ciciliano, M. N. Wells, A. M. Shah, K. F. Concannon, M. C. Donaldson, L. V. Sequist, E. Brachtel, D. Sgroi, J. Baselga, S. Ramaswamy, M. Toner, D. A. Haber, S. Maheswaran, *Science* **2013**, *339*, 580.

[13] a) L. S. Lim, M. Hu, M. C. Huang, W. C. Cheong, A. T. Gan, X. L. Looi, S. M. Leong, E. S. Koay, M. H. Li, *Lab Chip* **2012**, *12*, 4388; b) Y. Li, J. Guo, C. Wang, Z. Fan, G. Liu, Z. Gu, D. Damm, A. Mosig, X. Wei, *Cytometry Part A* **2011**, *79*, 848; c) O. Scatton, F. Chiappini, X. H. Liu, P. Riou, A. Marconi, B. Debuire, D. Azoulay, *J. Surg. Res.* **2008**, *150*, 183.

[14] a) J. Shao, J. Xue, Y. Dai, H. Liu, N. Chen, L. Jia, J. Huang, *Eur. J. Cancer* **2012**, *48*, 2086; b) J. Shao, Y. Dai, W. Zhao, J. Xie, J. Xue, J. Ye, L. Jia, *Cancer Lett.* **2013**, *330*, 49.

[15] J. Z. Chen, J. C. Wang, Y. Gao, R. J. Zeng, Z. Jiang, Y. W. Zhu, J. W. Shao, L. Jia, *J. Pharm. Biomed. Anal.* **2014**, *95*, 158.

[16] O. C. Farokhzad, J. Cheng, B. A. Teply, I. Sherifi, S. Jon, P. W. Kantoff, J. P. Richie, R. Langer, *Proc. Natl. Acad. Sci. U.S.A.* **2006**, *103*, 6315.

[17] F. S. Doekhie, H. Morreau, G. H. de Bock, F. M. Speetjens, N. G. Dekker-Ensink, H. Putter, C. J. van de Velde, R. A. Tollenaar, P. J. Kuppen, *Cancer Microenviron.* **2008**, *1*, 141.

[18] a) K. Pantel, M. Otte, *Semin. Cancer Biol.* **2001**, *11*, 327; b) V. Zieglschmid, C. Hollmann, O. Bocher, *Crit. Rev. Clin. Lab. Sci.* **2005**, *42*, 155.

[19] a) W. Sheng, O. O. Ogunwobi, T. Chen, J. Zhang, T. J. George, C. Liu, Z. H. Fan, *Lab Chip.* **2014**, *14*, 89; b) Q. Shen, L. Xu, L. Zhao, D. Wu, Y. Fan, Y. Zhou, W. H. Ouyang, X. Xu, Z. Zhang, M. Song, T. Lee, M. A. Garcia, B. Xiong, S. Hou, H. R. Tseng, X. Fang, *Adv. Mater.* **2013**, *25*, 2368; c) C. Y. Wen, L. L. Wu, Z. L. Zhang, Y. L. Liu, S. Z. Wei, J. Hu, M. Tang, E. Z. Sun, Y. P. Gong, J. Yu, D. W. Pang, *ACS Nano.* **2014**, *8*, 941.

[20] a) Y. Gao, J. Xie, H. Chen, S. Gu, R. Zhao, J. Shao, L. Jia, *Biotechnol. Adv.* **2014**, *32*, 761; b) S. Hong, P. R. Leroueil, I. J. Majoros, B. G. Orr, J. R. Baker Jr., M. M. Banaszak Holl, *Chem. Biol.* **2007**, *14*, 107.

[21] a) D. Pan, W. She, C. Guo, K. Luo, Q. Yi, Z. Gu, *Biomaterials* **2014**, *35*, 10080; b) N. Li, Q. Yi, K. Luo, C. Guo, D. Pan, Z. Gu, *Biomaterials* **2014**, *35*, 9529; c) C. Zhang, D. Pan, K. Luo, W. She, C. Guo, Y. Yang, Z. Gu, *Adv. Healthcare Mater.* **2014**, *3*, 1299; d) W. She, N. Li, K. Luo, C. Guo, G. Wang, Y. Geng, Z. Gu, *Biomaterials* **2013**, *34*, 2252; e) W. She, K. Luo, C. Zhang, G. Wang, Y. Geng, L. Li, B. He, Z. Gu, *Biomaterials* **2013**, *34*, 1613; f) N. G. Yabbarov, G. A. Posypanova, E. A. Vorontsov, O. N. Popova, E. S. Severin, *Biochemistry* **2013**, *78*, 884; g) A. F. Hussain, H. R. Kruger, F. Kampmeier, T. Weissbach, K. Licha, F. Kratz, R. Haag, M. Calderon, S. Barth, *Biomacromolecules* **2013**, *14*, 2510; h) M. H. Li, S. K. Choi, T. P. Thomas, A. Desai, K. H. Lee, A. Kotlyar, M. M. Banaszak Holl, J. R. Baker Jr., *Eur. J. Med. Chem.* **2012**, *47*, 560; i) C. Zhang, D. Pan, K. Luo, N. Li, C. Guo, X. Zheng, Z. Gu, *Polym. Chem.* **2014**, *5*, 5227.

[22] a) R. Shukla, T. P. Thomas, J. L. Peters, A. M. Desai, J. Kukowska-Latallo, A. K. Patri, A. Kotlyar, J. R. Baker, *Bioconjugate Chem.* **2006**, *17*, 1109; b) A. K. Patri, A. Myc, J. Beals, T. P. Thomas, N. H. Bander, J. R. Baker, *Bioconjugate Chem.* **2004**, *15*, 1174; c) T. P. Thomas, A. K. Patri, A. Myc, M. T. Myaing, J. Y. Ye, T. B. Norris, J. R. Baker Jr., *Biomacromolecules* **2004**, *5*, 2269.

[23] M. Balzar, M. J. Winter, C. J. de Boer, S. V. Litvinov, *J. Mol. Med.* **1999**, *77*, 699.

[24] a) J. Haier, M. Nasralla, G. L. Nicolson, *Ann. Surg.* **2000**, *231*, 11; b) K. Gunther, O. Dworak, S. Remke, R. Pfluger, S. Merkel, W. Hohenberger, M. A. Reymond, *J. Surg. Res.* **2002**, *103*, 68.

[25] a) E. Jan, N. A. Kotov, *Nano Lett.* **2007**, *7*, 1123; b) W. Kim, J. K. Ng, M. E. Kunitake, B. R. Conklin, P. Yang, *J. Am. Chem. Soc.* **2007**, *129*, 7228.

[26] R. Duncan, L. Izzo, *Adv. Drug Deliv. Rev.* **2005**, *57*, 2215.

[27] a) J. Ross, K. Gray, D. Schenkein, B. Greene, G. S. Gray, J. Shulok, P. J. Worland, A. Celniker, M. Rolfe, *Expert Rev. Anticancer Ther.* **2003**, *3*, 107; b) D. J. Slamon, B. Leyland-Jones, S. Shak, H. Fuchs, V. Paton, A. Bajamonde, T. Fleming, W. Eiermann, J. Wolter, M. Pegram, J. Baselga, L. Norton, *N. Engl. J. Med.* **2001**, *344*, 783.

[28] a) G. Sahay, D. Y. Alakhova, A. V. Kabanov, *J. Controlled Release* **2010**, *145*, 182; b) S. F. Peng, C. J. Su, M. C. Wei, C. Y. Chen, Z. X. Liao, P. W. Lee, H. L. Chen, H. W. Sung, *Biomaterials* **2010**, *31*, 5660.

[29] a) E. Ozkumur, A. M. Shah, J. C. Ciciliano, B. L. Emmink, D. T. Miyamoto, E. Brachtel, M. Yu, P. I. Chen, B. Morgan, J. Trautwein, A. Kimura, S. Sengupta, S. L. Stott, N. M. Karabacak, T. A. Barber, J. R. Walsh, K. Smith, P. S. Spuhler, J. P. Sullivan, R. J. Lee, D. T. Ting, X. Luo, A. T. Shaw, A. Bardia, L. V. Sequist, D. N. Louis, S. Maheswaran, R. Kapur, D. A. Haber, M. Toner, *Sci. Transl. Med.* **2013**, *5*, 179ra47; b) M. Mego, U. De Giorgi, S. Dawood, X. Wang, V. Valero, E. Andreopoulou, B. Handy, N. T. Ueno, J. M. Reuben, M. Cristofanilli, *Int. J. Cancer* **2011**, *129*, 417.

[30] Y. Lu, T. Yu, H. Liang, J. Wang, J. Xie, J. Shao, Y. Gao, S. Yu, S. Chen, L. Wang, L. Jia, *Sci. Rep.* **2014**, *4*, 4344.

[31] J. Wang, J. Chen, L. Wan, J. Shao, Y. Lu, Y. Zhu, M. Ou, S. Yu, H. Chen, L. Jia, *AAPS J.* **2014**, *16*, 289.